RSC Advances

PAPER

View Article Online
View Journal | View Issue

Cite this: *RSC Adv.*, 2018, **8**, 25268

Reaction of FcC≡CC(O)R (Fc = ferrocenyl) with $Ru_3(CO)_{12}$ leading to unexpected nitro-group reduced ruthenoles and 1,2-CO-inserted triruthenium clusters†

Lei Xu, Liping Jiang, Shasha Li, Guofang Zhang,* Weiqiang Zhang and Ziwei Gao

The reaction of $Ru_3(CO)_{12}$ with ferrocene-containing alkynyl ketones FcC≡CC(O)R (Fc = ferrocenyl; R = Ph (**1**); 2-thienyl (**2**); 4-CH_3O–Ph (**3**); 4-NH_2–Ph (**4**); 4-NO_2–Ph (**5**); ferrocenyl (**6**)) proceeds in toluene with the formation of triruthenium clusters (**1a–6a**), ruthenoles (**1b–5b**, **5c** and **1d–5d**) and unexpected 1,2-CO-inserted triruthenium clusters (**1c–4c**). **1a–6a** were isolated from the reaction of $Ru_3(CO)_{12}$ with one equivalent of **1–6**, respectively. Ruthenoles **1b–5b**, **5c** and **1d–5d** were collected by adding **1–5** to the corresponding **1a–5a** in a molar ratio of 1 : 1, respectively. Unexpectedly, the nitro group in one of the two phenyl rings in both **5c** and **5d** molecules was reduced to an amino group, while their ruthenole skeletons are retained. When **1–4** were added to the corresponding **1a–4a** in a molar ratio of 1 : 1, respectively, the unusual triruthenium clusters (**1c–4c**) were isolated, involving 1,2-insertion of a terminal coordinated carbonyl between two C≡C units of the ynone molecules. No reaction between **6a** and **6** was observed. And the familiar cyclotrimerization products were not found. All new compounds were characterized by NMR, FT-IR, and MS-ESI and most of them were structurally confirmed by single crystal X-ray diffraction. The results suggested that the ferrocenyl groups in the 1,3-ynones exhibit strong electron and steric effects on the reaction process and product distribution during their reactions with $Ru_3(CO)_{12}$.

Received 28th May 2018
Accepted 6th July 2018

DOI: 10.1039/c8ra04548h

rsc.li/rsc-advances

Introduction

$Ru_3(CO)_{12}$ as a potent catalyst precursor has attracted great interest of researchers due to its unique activity in homogeneous catalytic reactions.[1] It was usually used for activation and conversion of chemical bonds for the construction of diverse C–X (X = C, N, O, Si, *etc.*) bonds.[2] To understand the related activated mechanisms, reactions of $Ru_3(CO)_{12}$ with NHCs,[3] arenes,[4] alkenes[5] and alkynes[6] were extensively investigated. In recent years, some carbonyl ruthenium compounds formed *via* $Ru_3(CO)_{12}$ and unsaturated hydrocarbons have been used in catalytic reactions.[7] These reactions provide more possibilities for $Ru_3(CO)_{12}$ to become a potential catalyst for the conversion of alkyne compounds.

Ruthenium clusters containing alkyne-derived ligands have been studied for many years and a variety of coordination modes were reported.[8] The coordination patterns are usually relevant to many catalytic processes involving polynuclear species and unsaturated organic molecules.[9] Previously P. J. Low studied the reactions of $Ru_3(CO)_{12}$ with 1,6-bis(trimethylsilyl)-hexa-1,3,5-triyne and separated a series of Ru_2–Ru_4 clusters.[10] In the meantime, S. W. Lau synthesized ruthenium diyne clusters with diverse Ru-diyne coordination modes *via* reaction of $Ru_3(CO)_{12}$ with 1,4-bis(1-hydroxycyclopentyl)-1,3-butadiyne.[11] Then R. Rosseto systematically investigated the reaction of some asymmetrical alkynes with $Ru_3(CO)_{12}$ and revealed the electron effects of the groups in the aromatic ring(s).[12] M. Li reported the trinuclear complexes (3,4-$R_2C_5H_2)_2(\mu_3$-$C_4Ph_2)$ $Ru_3(CO)_6(\mu$-$CO)_2$ (R = Me, Ph) and the dinuclear complex (3,4-$Ph_2C_5H_2)_2(\mu$-$C_4Ph_2)Ru_2(CO)_5(\mu$-CO) by reaction of $Ru_3(CO)_{12}$ with $\{\eta^5$-[1,2-R_2-4-(PhC≡C)$C_5H_2]\}_2ZrCl_2$ (R = Me, Ph), *via* the unexpected cleavage of the two Cp–Zr bonds.[13] Recently, P. Mathur reported a series of [$Ru(CO)_3(\eta^4$-ruthenole)] derivatives during the reaction of $Ru_3(CO)_{12}$ with FcC_2C_2Ph (Fc = ferrocenyl).[14] Therefore, the reactions of

Key Laboratory of Applied Surface and Colloid Chemistry, MOE/School of Chemistry and Chemical Engineering, Shaanxi Normal University, Xi'an 710062, China. E-mail: gfzhang@snnu.edu.cn

† Electronic supplementary information (ESI) available: Crystal structures of **1d**, **2a**, **2b** and **4d**, DFT-optimized structures, calculated IR, NMR spectra and geometric parameters of **2c** and **5c**, CIF, checkcif, ^{1}H NMR spectra, ^{13}C NMR spectra, FT-IR spectra and other electronic format. CCDC 1833763 (**1b**), 1833764 (**1d**), 1833765 (**2a**), 1812864 (**2b**), 1836272 (**2c**), 1812871 (**2d**), 1833754 (**4a**), 1836273 (**4d**) and 1833755 (**5d**). For ESI and crystallographic data in CIF or other electronic format see DOI: 10.1039/c8ra04548h

$Ru_3(CO)_{12}$ with different acetylenes can afford a variety of unexpected products,[10–15] which motivates us to explore the activated mechanisms *via* experienced sophisticated transformations of alkynes.

Alkynyl ketones as important functional alkynes, are often employed as key templates in modern chemical synthesis.[16] For understanding reactive activity of 1,3-ynones with $Ru_3(CO)_{12}$, reactions of a few 1,3-diphenylprop-2-yn-1-one derivatives with $Ru_3(CO)_{12}$ have been systematically investigated in our recent studies, and a series of Ru_2–Ru_4 clusters were isolated.[17] After a detailed analysis of the results, we believed that, during the reaction of a 1,3-ynone with $Ru_3(CO)_{12}$, not only the group at its carbonyl side exerts effects on its reactivity and transformation process, but the group at its C≡C side influences the reaction direction as well. As a continuing work in the chemistry of $Ru_3(CO)_{12}$ with alkynyl ketones, we introduced a ferrocenyl group at the C≡C side of a 1,3-diphenylprop-2-yn-1-one derivative to substitute the phenyl group, and investigated the structures of the intermediates and final products during its reactions with $Ru_3(CO)_{12}$.

In this paper, we examined in detail the reaction processes of $Ru_3(CO)_{12}$ with six FcC≡CC(O)R (Fc = ferrocenyl; R = Ph (**1**); 2-thienyl (**2**); 4-CH_3O–Ph (**3**); 4-NH_2–Ph (**4**); 4-NO_2–Ph (**5**); ferrocenyl (**6**)) compounds. In the compounds **1–6**, the selected groups at their carbonyl sides are phenyl (**1**) and 2-thienyl (**2**) rings with no substituents, phenyl rings with electron-donating groups (**3** and **4**) and electron-withdrawing group (**5**), and a sterically hindered ferrocenyl group (**6**). The coordination and couplings of the alkynyl ketones with $Ru_3(CO)_{12}$ formed a series of ruthenium clusters. Through a detailed examination of the reaction processes, we found that the ferrocenyl groups in **1–6** play important roles in the reaction process and formation of the products. Compared with the studied 1,3-diphenylprop-2-yn-1-one derivatives,[17] the reactions of the ferrocene-containing 1,3-ynones **1–6** with $Ru_3(CO)_{12}$ afforded unexpected 1,2-CO-inserted π-coordinated triruthenium clusters (**1c–4c**), the head-to head ruthenoles (**5c** and **5d**) with reduction of half of the nitro groups into amino groups. The common cyclotrimerization products were not isolated, however.

Results and discussion

Syntheses and characterization

The thermal reactions of 1,3-ynones (**1–6**) with $Ru_3(CO)_{12}$ were carried out in toluene at 90 °C under nitrogen atmosphere. The reaction courses were monitored by TLC technique. After slow cooling, the unreacted $Ru_3(CO)_{12}$ was filtered and recovered, the solvents were removed and the residues were chromatographed on silica gel with dichloromethane and it was found that a mixture of ruthenium clusters was obtained. Although the yield of each product is low, the yield of the mixture in each reaction is not very low. If the recovered $Ru_3(CO)_{12}$ was taken into account, the recovery of the ruthenium in each reaction is substantially high. According to the experimental results, the product distribution was illustrated in Scheme 1.

Formation of the clusters $Ru_3(CO)_9(\mu_2\text{-CO})(\mu_3\text{-}\eta^1\text{:}\eta^2\text{:}\eta^1$-triruthenium) derivatives (**1a–6a**) were observed in the reactions of **1–6** with $Ru_3(CO)_{12}$ in toluene at 90 °C for 30 min. These clusters were formed by binding of the C≡C bonds of the 1,3-ynones with Ru metal skeletons. This reaction course was similar to that of $Ru_3(CO)_{12}$ with a 1,3-diphenylprop-2-yn-1-one derivative.[17] Since the molecular structures of **1a–6a** are similar, **4a**

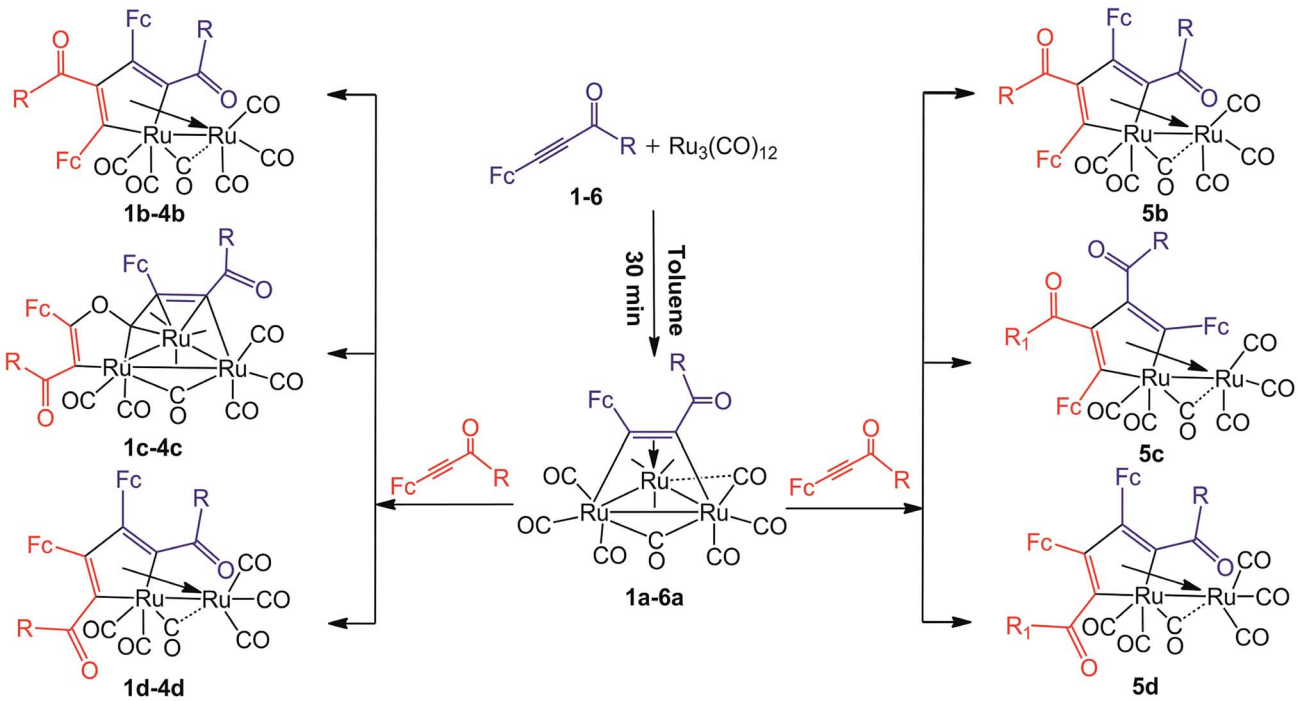

Scheme 1 The product distribution of $Ru_3(CO)_{12}$ with FcC≡CC(O)R (Fc = ferrocenyl) (**1–6**). R = Ph (**1**); 2-thienyl (**2**); 4-CH_3O–Ph (**3**); 4-NH_2–Ph (**4**); 4-NO_2–Ph (**5**); Fc (**6**).

was taken as an example, the FT-IR absorption in the range of 2011–2098 cm^{-1} and 1878 cm^{-1} were assigned to its terminal and bridging CO groups, respectively. The chemical shift of the C≡C bond moved downwards to 152.51 ppm, confirming a strong interaction between the C≡C bond and the three Ru atoms. Since the terminal and bridging CO groups are fluxional in solution, the carbonyl carbon atoms cannot be distinguished by $^{13}C\{1H\}$ NMR spectroscopy.

The structure of **4a** (Fig. 1) consists of a triangular arrangement of the three ruthenium atoms, in which the Ru–Ru bond distances are in the range of 2.7191(9)–2.8130(7) Å. The coordination of the alkynyl ketone with Ru_2 is in a η^2 mode, but with Ru_1 and Ru_3 is in a η^1 mode. The distances of Ru_1–C_{22} and Ru_2–C_{22} are 1.9143(36) and 2.9786(41) Å, respectively, indicative of the existence of a semi-bridging carbonyl group between Ru_1 and Ru_2 atoms. The C_{11}–C_{12} bond length is 1.3947(46) Å, which is between the typical C–C single bond and double bond and is elongated significantly.[18] The angle of Ru_1–C_{22}–O_4 is 172.534(310)°.

By increasing the reaction time of 1,3-ynones **1–5** with $Ru_3(CO)_{12}$ to 2 h, three types of the common $Ru(CO)_3(\eta^4$-ruthenole) derivatives **1b–5b**, **5c**, **1d–5d** and unusual 1,2-CO-inserted π-coordinated triruthenium clusters **1c–4c** were isolated. The structural characterizations showed that all ruthenoles each contains a metallacyclopentadienyl framework,[19] similar in structure to the corresponding ruthenoles we reported previously,[17] in which two 1,3-ynone molecules couple by the C≡C units in modes head-to-tail coupling (**1b–5b**), head-to-head coupling (**5c**) and tail-to-tail coupling (**1d–5d**).[17] Accordingly, we choose **1b** (Fig. 2) from **1b–5b** as an example to describe the molecular structures of these clusters. The structure of **1b** consists of five terminal and one semi-bridging carbonyls. The distance of the Ru–Ru bond is 2.7543(6) Å. The lengths of the C–C bonds [1.4380(41)–1.4439(39) Å] in the metallacyclopentadiene ($Ru_1C_{11}C_{12}C_{30}C_{31}$) reflect the interactions between the Ru_2 atom and the 1,3-ynone, and most of the Ru–C bond lengths related with the metallacyclopentadiene fall into two distinct ranges, 2.0851(29)–2.0920(28) Å and 2.2066(24)–2.2917(27) Å. In addition, the dihedral angles between Ru_1–Ru_2–$C_{42_{plane}}$ and Ru_1–Ru_2–$C_{39_{plane}}$, Ru_1–Ru_2–$C_{41_{plane}}$ are 58.4(2)° and 41.0(2)°, respectively.

Upon comparison the FT-IR, NMR and ESI-MS data of **5c** with those of the characterized ruthenoles, we proposed that **5c** has a similar structure to the ruthenoles with the head-to-head coupling mode of two 1,3-ynone molecules in our previous studies,[17] with the nitro group in one phenyl ring being reduced to an amino group. Since no single crystals suitable for single-crystal X-ray diffraction were grown for **5c**, DFT calculations were carried out to confirm the structure of **5c**. The optimized structure of **5c** and its calculated IR and NMR spectra are shown in Fig. S6,† NMR and FT-IR spectra in the ESI,† respectively. They showed that the calculated NMR and IR spectra of **5c** were consistent with its determined NMR and IR spectra, confirming the structure of **5c**.

Unexpectedly, the characterization results of **1c–4c** are completely different from those of the usual ruthenole such as **5c**. Fortunately, crystal structure of **2c** (ORTEP view of **2c** is displayed in Fig. S4†) was established, although the wR_2 in the crystal data of **2c** was larger than 0.15. Then we employed DFT

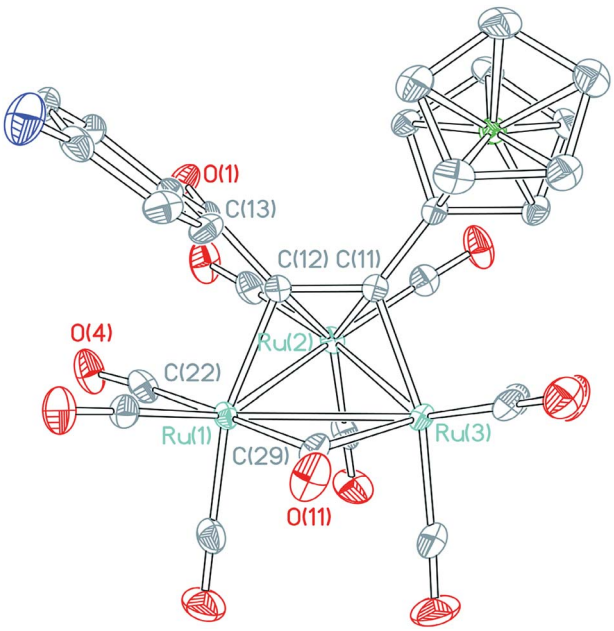

Fig. 1 ORTEP view of cluster **4a** showing 50% ellipsoids. Selected bond lengths (Å) and bond angles (°): Ru_1–Ru_2 = 2.7256(9); Ru_2–Ru_3 = 2.7191(9); Ru_1–Ru_3 = 2.8130(9); Ru_1–C_{22} = 1.9143(36); Ru_1–C_{29} = 2.1337(36); Ru_1–C_{12} = 2.1235(34); Ru_2–C_{11} = 2.2893(35); Ru_2–C_{12} = 2.2415(32); Ru_2–C_{22} = 2.9786(41); Ru_3–C_{11} = 2.1147(36); Ru_3–C_{29} = 2.1612(43); C_{11}–C_{12} = 1.3947(46); C_{12}–C_{13} = 1.4987(50); C_{13}–O_1 = 1.2258(44); C_{22}–O_4 = 1.1356(43); C_{29}–O_{11} = 1.1540(5); Ru_1–C_{22}–Ru_2 = 63.391(11); Ru_1–C_{29}–Ru_3 = 81.830(13).

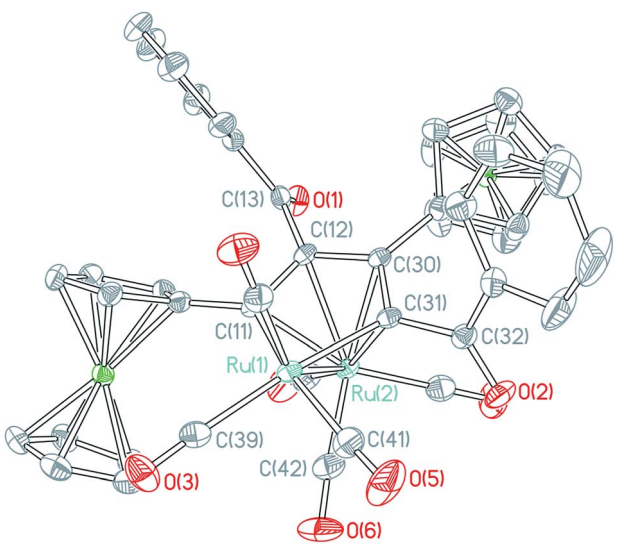

Fig. 2 ORTEP view of cluster **1b** showing 50% ellipsoids. Selected bond lengths (Å) and bond angles (°): Ru_1–Ru_2 = 2.7543(6); Ru_1–C_{11} = 2.0920(28); Ru_1–C_{31} = 2.0851(29); Ru_1–C_{39} = 1.9625(37); Ru_1–C_{42} = 2.7660(3); Ru_2–C_{11} = 2.2598(21); Ru_2–C_{12} = 2.2809(24); Ru_2–C_{31} = 2.2066(24); Ru_2–C_{30} = 2.2917(27); Ru_2–C_{42} = 1.8989(45); C_{11}–C_{12} = 1.4394(43); C_{12}–C_{30} = 1.4439(39); C_{30}–C_{31} = 1.4380(41); C_{31}–C_{32} = 1.4877(39); C_{32}–O_2 = 1.2215(30); C_{12}–C_{13} = 1.5148(44); C_{13}–O_1 = 1.2166(39); Ru_1–C_{42}–Ru_2 = 69.550(12); Ru_2–C_{42}–O_6 = 168.948(34).

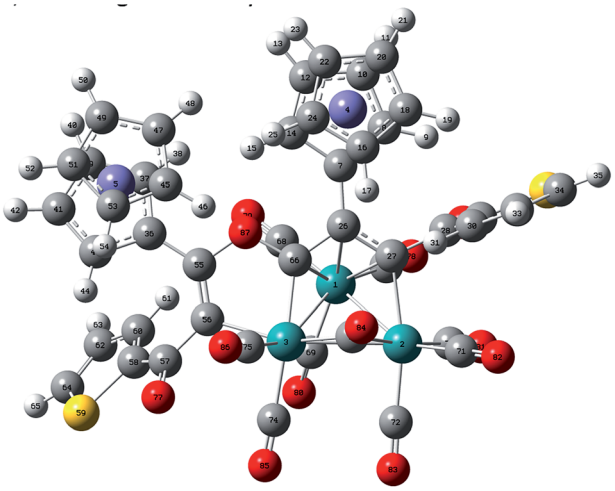

Fig. 3 DFT-optimized structure of **2c** at the level of B3LYP/LanL2DZ/6-31G. Selected bond lengths (Å) and bond angles (°): Ru_1–Ru_2 = 2.8093, Ru_2–Ru_3 = 2.9157, Ru_1–Ru_3 = 2.9325, Ru_1–C_{26} = 2.4356, Ru_1–C_{66} = 2.3153, Ru_1–C_{27} = 2.2934, Ru_2–C_{73} = 2.1992, Ru_3–C_{56} = 2.1019, Ru_3–C_{73} = 2.0764, Ru_3–C_{66} = 2.0405, C_{26}–C_{27} = 1.4355, C_{26}–C_{66} = 1.4693, C_{66}–O_{87} = 1.4052, C_{55}–O_{87} = 1.4032, C_{55}–C_{56} = 1.3601, C_{56}–C_{57} = 1.4786, C_{57}–O_{77} = 1.2621, C_{27}–C_{28} = 1.4937, C_{28}–O_{76} = 1.2599, Ru_2–C_{73}–Ru_3 = 85.9399, Ru_3–C_{66}–O_{87} = 113.3175, Ru_3–C_{66}–C_{26} = 131.1049.

calculations to verify its structure. The calculated molecular structure of **2c** (shown in Fig. 3) is identical to the established one, indicating that the crystal structure of **2c** is correct.

Although a similar skeleton to the structure of **2c** has been reported in the reaction of $Os_3(CO)_{10}(MeCN)_2$ with terminal acetylene ligands,[20] this type of structure formed by ruthenium atoms has never been reported until now. The structure of **2c** consists of a triangular arrangement of the ruthenium atoms with the Ru–Ru bond distances in the range of 2.7681(17)–2.8236(16) Å. Two 1,3-ynone molecules are coupled by the 1,2-insertion of a terminal coordinated CO molecule in two carbon–carbon triple bonds. The dimerized 1,3-ynone ligands are bound to the triruthenium core by three σ-bonds Ru_1–C_{11}, Ru_1–C_{12} and Ru_1–C_{35} and its allyl moiety $C_{11}C_{12}C_{35}$ is π-coordinated by the Ru_1 atom. Two five-membered cycles $Ru_3C_{35}O_3C_{28}C_{29}$ and $Ru_2C_{12}C_{11}C_{35}Ru_3$ are fused *via* the Ru_3–C_{35} bond and do not display considerable deviations from planarity (maximum deviations from their mean planes are 0.2187(16) and 0.1013(16) Å, respectively), the dihedral angle formed by their planes is equal to 24.415(34)°. The angles of Ru_3–C_{35}–O_3, C_{11}–C_{35}–O_3 and Ru_3–C_{35}–C_{11} are 115.182(10)°, 116.011(13)° and 128.792(11)°, respectively.

The molecular structures of ruthenoles **1d–5d** (tail-to-tail coupling mode) are similar, therefore the structures of both **2d** and **5d**·CH_2Cl_2 are taken as examples and their ORTEP views are shown in Fig. 4 and 5. The distances of the Ru–Ru bonds in **2d** and **5d**·CH_2Cl_2 are 2.7285(3) and 2.7504(3) Å, respectively, and the differences between most of the Ru–C bond distances and of the C–C bond lengths bound with the Ru atoms are within a small ranges, a similar semi-bridging carbonyl group existed between two Ru atoms. In structure of **2d** the angle between C_{29}–C_{28}–C_{11}–C_{12} plane and Ru_1–Ru_2 is 39.145°, and the

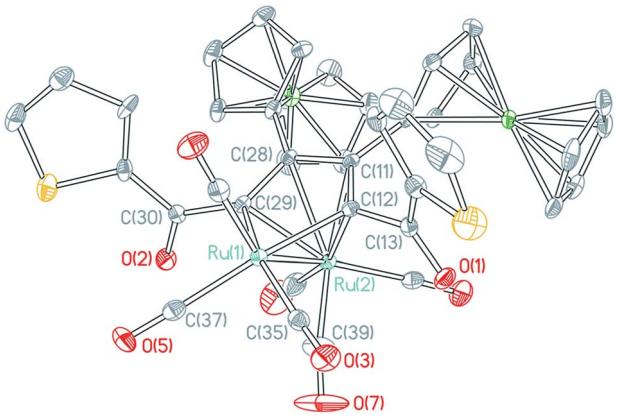

Fig. 4 ORTEP view of clusters **2d** showing 50% ellipsoids. Selected bond lengths (Å) and bond angles (°): Ru_1–Ru_2 = 2.7285(3); Ru_1–C_{29} = 2.0860(28); Ru_1–C_{12} = 2.0873(25); Ru_1–C_{39} = 2.7101(30); Ru_2–C_{29} = 2.2053(25); Ru_2–C_{28} = 2.3248(24); Ru_2–C_{11} = 2.2914(21); Ru_2–C_{12} = 2.2319(22); Ru_2–C_{39} = 1.9039(34); C_{28}–C_{29} = 1.4275(36); C_{28}–C_{11} = 1.4661(39); C_{11}–C_{12} = 1.4210(37); C_{12}–C_{13} = 1.4877(40); C_{29}–C_{30} = 1.4862(39); C_{13}–O_1 = 1.2272(34); C_{30}–O_2 = 1.2328(27); Ru_2–C_{39}–O_7 = 167.362(29); Ru_1–C_{39}–Ru_2 = 70.028(10).

angle between C_{31}–C_{30}–C_{11}–C_{12} plane and Ru_1–Ru_2 in **5d** is 39.882°, which are significantly different from that in the rhodium compound $(\eta\text{-}C_5H_5)_2Rh_2(\mu\text{-}CO)\{\mu\text{-}\eta^2{:}\eta^2\text{-}C(CF_3)H{=}C(CF_3)CMe{=}CH_2\}$ reported by R. S. Dickson.[21] Although, the cluster **5d**·CH_2Cl_2 has a similar skeleton structure to **1d–4d**, but in the molecule **5d**·CH_2Cl_2 a nitro group at the *para* position of a phenyl ring was reduced to an amino group, as encountered in **5c**. Its NMR, FT-IR and MS spectra support the existence of the amino group.

Transformation process from 1,3-ynones to final products

The reaction of $Ru_3(CO)_{12}$ with ferrocene-containing 1,3-ynones (**1–6**) were studied in detail. Experimental results show that the reaction processes during the formation of **1a–**

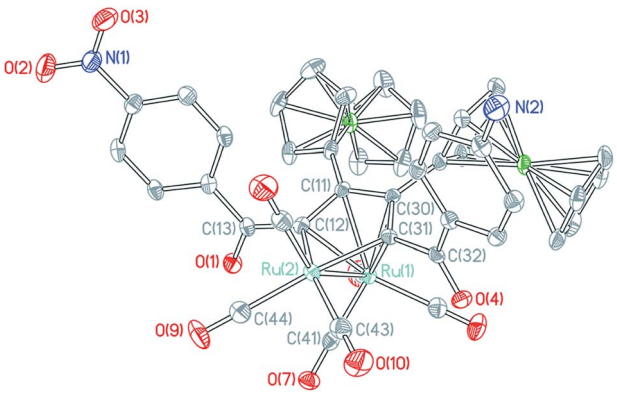

Fig. 5 ORTEP view of clusters **5d**·CH_2Cl_2 showing 50% ellipsoids (solvent molecules have been omitted for clarity). Selected bond lengths (Å) and bond angles (°): Ru_1– Ru_2 = 2.7504(3); Ru_1–C_{41} = 1.9080(24); Ru_2–C_{41} = 2.8071(24); Ru_2–C_{12} = 2.0928(22); Ru_2–C_{31} = 2.0811(23); C_{11}–C_{12} = 1.4275(32); C_{11}–C_{30} = 1.4611(30); C_{30}–C_{31} = 1.4274(31); C_{31}–C_{32} = 1.4954(30); C_{32}–O_4 = 1.2316(28); C_{12}–C_{13} = 1.4829(31); C_{13}–O_1 = 1.2280(28); Ru_1–C_{41}–O_7 = 173.338(21); Ru_1–C_{41}–Ru_2 = 68.331(62).

6a were similar to those reported in our work earlier.[17] However, the successive reaction of **1a–6a** with the corresponding **1–6** afforded some unexpected products, but gave no anticipated cyclotrimerization products. According to the explanation that an electron-withdrawing group activates an alkyne and meanwhile an electron-donating group deactivates an alkyne,[22] the larger steric hindrance and electron-donating property of two ferrocenyl groups in **6** results in the formation of **6a** as the unique product in the reaction of **6** with $Ru_3(CO)_{12}$. Meanwhile, no cyclotrimerization products of the 1,3-ynones were formed, due mainly to the lower activity of the alkynyl ketones in the presence of ferrocenyl groups.

Moreover, we also found that formation of the final products has been governed jointly by the electronic properties of both groups at both sides of the C≡C unit of a 1,3-ynone. For example, **5** has a strong electron-withdrawing *para*-nitrophenyl group at its carbonyl side, its reaction with **5a** can afford ruthenole derivatives **5b**, **5c** and **5d**. However, in both **5c** and **5d**, it is noted that one of the two nitro groups in each molecule is reduced to an amino group. A. Bassoli and A. Thurkauf reported that nitro groups of nitrobenzene derivatives can be reduced by CO to amino groups in the presence of catalytic amounts of $Ru_3(CO)_{12}$.[23] M. Lauwiner also approved that electron-withdrawing and/or weak electron-donating groups on the azo bridge at *para* position of nitrobenzene derivatives is beneficial to nitro group reduction in 4-nitrophenylazobenzenes by hydrazine hydrate in the presence of iron oxide/hydroxide catalyst.[24] Therefore, we supported that the reduction of nitro groups in the phenyl rings of **5c** and **5d** was accelerated by CO, with $Ru_3(CO)_{12}$ as catalyst, and the electron-donating ferrocenyl group. During the reaction of 1-(4-nitrophenyl)-3-phenylprop-2-yn-1-one with $Ru_3(CO)_{12}$, the strong electron-donating property of the phenyl ring leads to the retaining of the nitro groups in the corresponding ruthenoles.[17b]

In the case of the reaction of **1a–4a** with the corresponding alkynyl ketone **1–4**, no common head-to-head coupled ruthenole was found, the rare 1,2-CO-inserted π-coordinated triruthenium cluster **1c–4c** were formed instead. We noted that there are no electron-withdrawing groups at the carbonyl sides of these alkynyl ketones. We surmised that electron effect plays a significant role in the reaction directing, taking **2c** as an example: the 2-thienyl group is an electron-donating group and thus increases the electron density of the C≡C bond and deactivates the reactivity of the C≡C bond with Ru_3 in some degree, C_{28} of the C≡C bond does not link in this case with Ru_3, instead bonds with O_3 of the terminal CO coordinated with Ru_3, and C_{35} of the CO inserts between the C_{11} and Ru_3 bond, thus finishing the 1,2-insertion of the CO group in the two 1,3-ynone molecules, forming the $C_{35}C_{11}C_{12}$ π-coordinated triruthenium cluster **2c**.

Experimental

General procedures

All reactions and manipulations were performed under dry high-purity nitrogen using standard Schlenk techniques. $Ru_3(CO)_{12}$ and **1–6** were synthesized according to the literature procedures.[25] The solvents used in the experiments were purified, dried and distilled from sodium under a nitrogen atmosphere prior to use. Preparative TLC was performed on 20 × 20 cm glass plates coated with silica gel (Merck GF254, 0.5 mm thick). FT-IR spectra were recorded on a Bruker Tensor 27 Fourier-transform spectrometer. ^{1}H and ^{13}C{1H} NMR spectra were performed on a Bruker Avance 400 MHz spectrometer unless indicated. ESI was recorded on a Thermo DecaMax (LC-MS) mass spectrometer with an ion-trap mass detector. While high-resolution mass spectra were recorded in ESI mode on a Waters UPLC-Q-TOF mass spectrometer.

Synthesis

1-Phenyl-3-ferrocenyl-2-yn-1-one (**1**), 1-(2-thienyl)-3-ferrocenyl-2-yn-1-one (**2**), 1-(4-methoxy-phenyl)-3-ferrocenyl-2-yn-1-one (**3**), 1-(4-amino-phenyl)-3-ferrocenyl-2-yn-1-one (**4**), 1-(4-nitro-phenyl)-3-ferrocenyl-2-yn-1-one (**5**) and 1,3-ferrocenyl-2-yn-1-one (**6**) were used to react with $Ru_3(CO)_{12}$. Since the reaction processes are similar, taking reaction procedure of **1** with $Ru_3(CO)_{12}$ as an example. Both **1** (0.1856 g, 0.9 mmol) and $Ru_3(CO)_{12}$ (0.1918 g, 0.3 mmol) were added in 15 mL toluene and heated at 90 °C for 30 min, it was found that color of each reaction solution gradually changed from red-brown to black. The black solution was cooled and the unreacted orange-red $Ru_3(CO)_{12}$ was precipitated and recovered (0.697 g). The residue was chromatographed by 305 mm length and 32 mm internal diameter chromatographic column on silica gel with dichloromethane and petroleum ether. The main products were eluted in the sequence of **1a**, **1b**, **1c** and **1d** with the eluent being dichloromethane/petroleum ether (v/v) 1 : 10, 1 : 4, 1 : 3 and 1 : 1, respectively. And then the products were recrystallized by dichloromethane and hexane. The yields of the clusters **1a**, **1b**, **1c** and **1d** were calculated based on the added $Ru_3(CO)_{12}$ in the beginning of the reaction.

[$Ru_3(CO)_9(\mu_2$-CO){μ_3-η^1:η^2:η^1-(Ph)C(O)CC(Fc)}] (1a). Red-brown powder. Yield: 8%. FT-IR (KBr, cm^{-1}): 3095 w, 2962 w, 2926 w, 2852 w, 2099 s, 2056 vs, 2028 vs, 2002 vs, 1962 s, 1860 m. ^{1}H NMR (400 MHz, $CDCl_3$) δ 8.18–8.20 (dd, 2H, C_6H_5), 7.53–7.55 (m, 3H, C_6H_5), 3.88–4.10 (m, 9H, $C_{10}H_9$). ^{13}C{1H} NMR (101 MHz, $CDCl_3$) δ 195.26 (CO), 166.77, 166.69 (C≡C), 132.24, 129.62, 127.59 (C_6H_5), 94.43, 68.67 ($C_{10}H_9$). MS (*m*/*z*, ESI−) 901.792 (M−). Anal. calcd for $C_{29}H_{14}O_{11}FeRu_3$: 901.702.

[$Ru(CO)_3${μ_4-η^1:η^2:η^1:η^1(PhC(O))CC(Fc)C(PhC(O))C(Fc)Ru(CO)$_3$} μ-CO] (1b). Red-brown powder. Yield: 15%. FT-IR (KBr, cm^{-1}): 3092 w, 2081 vs, 2053 vs, 2010 vs, 1982 vs. ^{1}H NMR (400 MHz, $CDCl_3$) δ 7.93–7.94 (d, 2H, C_6H_5), 7.77–7.78 (d, 2H, C_6H_5), 7.30–7.58 (m, 6H, C_6H_5), 3.67–4.04 (m, 18H, $C_{10}H_9$). ^{13}C{1H} NMR (101 MHz, $CDCl_3$) δ 197.26, 196.56, 196.06, 193.98, 193.72, 193.33 (CO), 164.65 (C≡C), 136.31, 135.58, 134.81, 133.73, 132.43, 129.58, 129.33, 128.89, 128.48, 128.03 (C_6H_5), 81.90, 75.61, 71.21, 70.72, 70.24, 69.72, 68.63, 68.56, 68.52, 68.42, 68.18, 67.49 ($C_{10}H_9$). MS (*m*/*z*, ESI−) 998.860 (M−). Anal. calcd for $C_{44}H_{28}O_8Fe_2Ru_2$: 998.858.

[$Ru_3(CO)_9$(μ-CO){μ_2-η^1:η^1-PhC(O)CC(Fc)}OC{μ_3-η^1:η^2-(Fc)CCC(O)Ph}] (1c). Black powder. Yield: 13%. FT-IR (KBr, cm^{-1}): 3090 w, 2924 w, 2849 w, 2099 vs, 2060 vs, 2036 vs, 2008 vs, 1998 s, 1858 m. ^{1}H NMR (400 MHz, $CDCl_3$) δ 7.77–8.19 (m, 4H, C_6H_5), 7.30–7.62 (m, 6H, C_6H_5), 3.67–4.90 (m, 18H, $C_{10}H_9$). ^{13}C

{1H} NMR (101 MHz, $CDCl_3$) δ 216.67, 203.50, 198.49, 197.25, 195.72, 195.05, 189.09, 184.19 (CO), 164.07 (C≡C), 137.18, 136.76, 136.55, 133.72, 133.29, 133.17, 132.94, 132.85, 132.42, 129.63, 129.58, 129.33, 128.91, 128.62, 128.55, 128.17, 128.03, 114.67 (C_6H_5), 82.35, 76.27, 71.88, 71.21, 70.72, 70.24, 70.15, 70.07, 70.01, 69.70, 69.44, 68.80, 68.74, 68.18, 67.85, 67.61, 67.49, 67.20 ($C_{10}H_9$). MS (*m*/*z*, ESI−) 1215.747 (M−). Anal. calcd for $C_{48}H_{28}O_{12}Fe_2Ru_3$: 1215.742.

[Ru(CO)$_3${μ_4-η^1:η^2:η^1:η^1(Fc)CC(PhC(O))C(PhC(O))C(Fc)Ru(CO)$_3$} μ-CO] (1d). Red-brown powder. Yield: 17%. FT-IR (KBr, cm^{-1}): 3100 w, 3008 w, 2961 w, 2925 w, 2849 w, 2086 vs, 2054 vs, 2027 vs, 2011 vs, 1985 vs, 1637 m. ^{1}H NMR (400 MHz, $CDCl_3$) δ 8.01–8.03 (d, 4H, C_6H_5), 7.46–7.56 (m, 6H, C_6H_5), 4.22 (s, 2H, $C_{10}H_9$), 4.15 (s, 2H, $C_{10}H_9$), 4.02 (s, 2H, $C_{10}H_9$), 3.96 (s, 2H, $C_{10}H_9$), 3.92 (s, 10H, $C_{10}H_9$). ^{13}C{1H} NMR (101 MHz, $CDCl_3$) δ 195.56, 195.05, 194.83, 193.14 (CO), 168.46 (C≡C), 135.61, 132.69, 130.14, 128.91, 128.04, 124.38 (C_6H_5), 84.26, 77.34, 77.02, 76.70, 74.28, 71.58, 70.40, 68.73, 68.55, 67.58 ($C_{10}H_9$). MS (*m*/*z*, ESI−) 998.851 (M−). Anal. calcd for $C_{44}H_{28}O_8Fe_2Ru_2$: 998.858.

[Ru$_3$(CO)$_9$(μ_2-CO){μ_3-η^1:η^2:η^1-(2-C_4H_3SC(O))CC(Fc)}] (2a). Red-brown powder. Yield: 9%. FT-IR (KBr, cm^{-1}): 3090 w, 2923 w, 2100 s, 2056 vs, 2021 vs, 2004 vs, 1962 s, 1849 m. ^{1}H NMR (400 MHz, $CDCl_3$) δ 7.98–7.99 (t, 1H, C_4H_3S), 7.75–7.76 (dd, 1H, C_4H_3S), 7.29–7.31 (m, 1H, C_4H_3S), 3.97–4.23 (m, 10H, $C_{10}H_9$). ^{13}C{1H} NMR (101 MHz, $CDCl_3$) δ 190.30 (CO), 169.94, 164.33 (C≡C), 141.29, 134.18, 133.98, 128.12 (C_4H_3S), 95.01, 70.35, 69.70, 68.80, 67.44 ($C_{10}H_9$). MS (*m*/*z*, ESI−) 906.659 (M−). Anal. calcd for $C_{27}H_{12}SO_{11}FeRu_3$: 906.660.

[Ru(CO)$_3${μ_4-η^1:η^2:η^1:η^1-(2-C_4H_3SC(O))CC(Fc)C(2-C_4H_3SC(O))C(Fc)Ru(CO)$_3$}μ-CO] (2b). Red-brown powder. Yield: 13%. FT-IR (KBr, cm^{-1}): 3060 w, 2088 vs, 2056 vs, 2017 vs, 1896 vs, 1409 m. ^{1}H NMR (400 MHz, $CDCl_3$) δ 7.68–7.70 (dd, 1H, C_4H_3S), 7.44–7.49 (m, 2H, C_4H_3S), 7.25–7.27 (m, 1H, C_4H_3S), 7.07–7.10 (m, 1H, C_4H_3S), 6.92–6.95 (m, 1H, C_4H_3S), 3.79–4.16 (m, 18H, $C_{10}H_9$). ^{13}C{1H} NMR (101 MHz, $CDCl_3$) δ 197.03, 196.00, 194.00, 193.12, 190.29, 185.92 (CO), 165.57, 158.05 (C≡C), 144.57, 142.28, 135.11, 134.26, 133.84, 133.13, 132.81, 128.97, 128.56, 127.68 (C_4H_3S), 97.06, 81.67, 76.00, 71.19, 70.97, 70.32, 69.83, 68.70, 68.53, 68.45, 68.24, 68.02, 67.69 ($C_{10}H_9$). MS (*m*/*z*, ESI−) 1010.771 (M−). Anal. Calcd for $C_{40}H_{24}S_2O_8Fe_2Ru_2$: 1010.771.

[Ru$_3$(CO)$_9$(μ-CO){μ_2-η^1:η^1-(2-C_4H_3SC(O))CC(Fc)}OC{μ_3-η^1:η^2-(Fc)CC(2-C_4H_3SC(O))}] (2c). Black powder. Yield: 11%. FT-IR (KBr, cm^{-1}): 3093 w, 2927 w, 2851 w, 2101 vs, 2061 vs, 2030 vs, 2010 vs, 1848 m. ^{1}H NMR (400 MHz, $CDCl_3$) δ 7.76–7.78 (d, 1H, C_4H_3S), 7.70 (s, 1H, C_4H_3S), 7.56–7.57 (dd, 1H, C_4H_3S), 7.41–7.42 (d, 1H, C_4H_3S), 7.25–7.25 (t, 1H, C_4H_3S), 6.98–7.00 (t, 1H, C_4H_3S), 4.78–4.80 (d, 2H, $C_{10}H_9$), 4.65–4.66 (d, 1H, $C_{10}H_9$), 4.15–4.40 (m, 15H, $C_{10}H_9$). ^{13}C{1H} NMR (101 MHz, $CDCl_3$) δ 195.61, 190.71, 188.75 (CO), 164.99 (C≡C), 143.92, 135.97, 134.15, 133.99, 133.08, 128.39, 128.21 (C_4H_3S), 82.65, 76.18, 71.77, 70.16, 69.71, 69.55, 69.12, 68.82, 68.66, 68.05 ($C_{10}H_9$). MS (*m*/*z*, ESI−) 1226.659 (M−). Anal. calcd for $C_{44}H_{24}S_2O_{12}Fe_2Ru_3$: 1226.656.

[Ru(CO)$_3${μ_4-η^1:η^2:η^1:η^1-(Fc)CC(2-C_4H_3SC(O))C(2-C_4H_3SC(O))C(Fc)Ru(CO)$_3$}μ-CO] (2d). Red-brown powder. Yield: 17%. FT-IR (KBr, cm^{-1}): 3095 w, 2924 w, 2952 w, 2847 w, 2086 vs, 2054 vs, 2023 vs, 1999 vs, 1960 s, 1603 m, 1406 s. ^{1}H NMR (400 MHz, $CDCl_3$) δ 7.59–7.64 (m, 4H, C_4H_3S), 7.12–7.14 (m, 2H, C_4H_3S), 3.97–4.22 (m, 18H, $C_{10}H_9$). ^{13}C{1H} NMR (101 MHz, $CDCl_3$) δ 195.20, 192.97, 189.01 (CO), 164.99 (C≡C), 143.78, 133.41, 127.71, 124.81 (C_4H_3S), 83.76, 74.35, 72.00, 70.41, 69.83, 68.46, 67.67 ($C_{10}H_9$). MS (*m*/*z*, ESI−) 1010.763 (M−). Anal. calcd for $C_{40}H_{24}S_2O_8Fe_2Ru_2$: 1010.771.

[Ru$_3$(CO)$_9$(μ_2-CO){μ_3-η^1:η^2:η^1-(Fc)CC(4-CH_3O-PhC(O))}] (3a). Red-brown powder. Yield: 11%. FT-IR (KBr, cm^{-1}): 3091 w, 2961 w, 2926 w, 2842 w, 2099 s, 2051 vs, 2019 vs, 1853 m. ^{1}H NMR (400 MHz, $CDCl_3$) δ 8.23–8.26 (d, 2H, C_6H_4), 7.11–7.13 (d, 2H, C_6H_4), 4.15–4.25 (m, 4H, $C_{10}H_9$), 4.01 (s, 5H, $C_{10}H_9$), 3.95 (s, 3H, CH_3O–). ^{13}C{1H} NMR (101 MHz, $CDCl_3$) δ 196.79 (CO), 170.31, 169.02 (C≡C), 165.00, 134.29, 127.36, 115.22 (C_6H_4), 96.99, 71.93, 71.09, 70.82, 70.52 ($C_{10}H_9$), 57.04 (CH_3O–). MS (*m*/*z*, ESI−) 930.715 (M−). Anal. calcd for $C_{30}H_{16}O_{12}FeRu_3$: 930.715.

[Ru(CO)$_3${μ_4-η^1:η^2:η^1:η^1-(4-CH_3O-PhC(O))CC(Fc)C(4-CH_3O-PhPhC(O))C(Fc)Ru(CO)$_3$}μ-CO] (3b). Red-brown powder. Yield: 18%. FT-IR (KBr, cm^{-1}): 3091 w, 2960 w, 2928 w, 2842 w, 2081 vs, 2053 vs, 2014 vs, 1982 vs, 1594 s. ^{1}H NMR (400 MHz, $CDCl_3$) δ 7.90–7.92 (d, 2H, C_6H_4), 7.77–7.75 (d, 2H, C_6H_4), 6.95–6.97 (d, 2H, C_6H_4), 6.81–6.83 (d, 2H, C_6H_4), 3.98–4.25 (m, 18H, $C_{10}H_9$), 3.75–3.94 (m, 6H, CH_3O–). ^{13}C{1H} NMR (101 MHz, $CDCl_3$) δ 198.96, 197.74, 197.04, 195.52, 194.91, 193.52 (CO), 165.43, 165.27, 164.25 (C≡C), 137.75, 133.15, 133.01, 131.24, 129.88, 129.25, 115.58, 114.71 (C_6H_4), 98.72, 83.34, 76.98, 72.46, 72.14, 71.96, 71.66, 71.12, 70.84, 70.04, 69.91, 69.78, 69.51, 68.85 ($C_{10}H_9$), 57.00, 56.80 (CH_3O–). MS (*m*/*z*, ESI−) 1058.872 (M−). Anal. calcd for $C_{46}H_{32}O_{10}Fe_2Ru_2$: 1058.879.

[Ru$_3$(CO)$_9$(μ-CO){μ_2-η^1:η^1-(4-CH_3O-PhC(O))CC(Fc)}OC{μ_3-η^1:η^2 -(Fc)CC(4-CH_3O-PhC(O))}] (3c). Black powder. Yield: 15%. FT-IR (KBr, cm^{-1}): 3091 w, 2964 w, 2930 w, 2852 w, 2097 vs, 2053 vs, 2007 vs, 1987 vs, 1853 m, 1595 s. ^{1}H NMR (400 MHz, $CDCl_3$) δ 7.74–7.92 (m, 4H, C_6H_4), 6.81–7.03 (m, 4H, C_6H_4), 3.95–4.36 (m, 18H, $C_{10}H_9$), 3.74–3.90 (m, 6H, CH_3O–). ^{13}C{1H} NMR (101 MHz, $CDCl_3$) δ 198.96, 198.53, 197.74, 197.29, 197.04, 195.77, 193.52, 192.23, 190.67 (CO), 166.05, 165.27, 164.88, 164.80, 164.53, 164.25 (C≡C), 138.24, 137.75, 133.42, 133.34, 133.15, 133.00, 131.40, 131.23, 131.03, 129.88, 129.24, 115.76, 115.30, 114.70 (C_6H_4), 98.71, 83.78, 83.33, 77.69, 76.97, 73.39, 72.45, 72.13, 71.65, 71.48, 71.39, 71.12, 70.84, 70.71, 70.15, 70.09, 70.03, 69.91, 69.81, 69.77, 69.51, 69.15, 68.85 ($C_{10}H_9$), 57.02, 56.84 (CH_3O–). MS (*m*/*z*, ESI−) 1273.763 (M−). Anal. calcd for $C_{50}H_{32}O_{14}Fe_2Ru_3$: 1273.763.

[Ru(CO)$_3${μ_4-η^1:η^2:η^1:η^1-(Fc)CC(4-CH_3O-PhC(O))C(4-CH_3O-PhC(O))C(Fc)Ru(CO)$_3$}μ-CO] (3d). Red-brown powder. Yield: 17%. FT-IR (KBr, cm^{-1}): 3095 w, 2934 w, 2840 w, 2086 vs, 2056 vs, 2016 vs, 1598 s. 1H NMR (400 MHz, $CDCl_3$) δ 7.84–8.01 (m, 4H, C_6H_4), 6.95–7.03 (m, 4H, C_6H_4), 3.95–4.29 (m, 18H, $C_{10}H_9$), 3.89 (s, 6H, CH_3O–). ^{13}C{1H} NMR (101 MHz, $CDCl_3$) δ 197.29, 196.70, 195.49, 194.76, 192.22 (CO), 170.44, 164.45 (C≡C), 133.71, 133.42, 130.10, 125.78, 115.76, 114.67 (C_6H_4), 85.66, 75.68, 72.98, 71.83, 71.48, 71.12, 69.89, 68.92 ($C_{10}H_9$), 56.89 (CH_3O–). MS (*m*/*z*, ESI−) 1058.873 (M−). Anal. Calcd for $C_{46}H_{32}O_{10}Fe_2Ru_2$: 1058.879.

[Ru$_3$(CO)$_9$(μ_2-CO){μ_3-η^1:η^2:η^1-(Fc)CC(4-NH_2-PhC(O))}] (4a). Red-brown powder. Yield: 7%. FT-IR (KBr, cm^{-1}): 3455 w, 3355

w, 2098 s, 2059 vs, 2011 s, 1857 s. ^{1}H NMR (400 MHz, $CDCl_3$) δ 8.04–8.11 (m, 2H, C_6H_4), 6.81–6.83 (d, 2H, C_6H_4), 6.72–6.74 (d, 2H, –NH_2), 4.20–4.73 (m, 18H, $C_{10}H_9$). ^{13}C{1H} NMR (101 MHz, $CDCl_3$) δ 194.37, 194.29 (CO), 152.51 (C≡C), 134.79, 134.54, 133.73, 133.26, 124.59, 122.10, 116.73, 115.17 (C_6H_4), 83.51, 71.84, 71.44, 71.26, 71.08, 70.82, 70.49, 69.74 ($C_{10}H_9$). MS (*m*/*z*, ESI−) 915.715 (M−). Anal. calcd for $C_{29}H_{15}NO_{11}FeRu_3$: 915.715.

[Ru(CO)$_3${μ$_4$-η^1:η^2:η^1:η^1-(4-NH$_2$-PhC(O))CC(Fc)C(4-NH$_2$-PhC(O))C(Fc)Ru(CO)$_3$}μ-CO] (4b). Red-brown powder. Yield: 12%. FT-IR (KBr, cm^{-1}): 3460 m, 3369 m, 2917 w, 2846 w, 2092 s, 2056 vs, 2025 s, 2009 s, 1852 m, 1593 s. ^{1}H NMR (400 MHz, $CDCl_3$) δ 7.70–7.72 (d, 4H, C_6H_4), 6.81 (s, 4H, –NH_2), 6.59–6.72 (dd, 4H, C_6H_4), 4.24–4.94 (m, 18H, $C_{10}H_9$). ^{13}C{1H} NMR (101 MHz, $CDCl_3$) δ 192.21, 191.83 (CO), 168.55, 165.21, 161.54 (C≡C), 133.62, 128.92, 121.47, 115.50, 115.41 (C_6H_4), 72.03, 72.02, 71.81, 71.77, 71.46, 71.43, 71.35, 71.34, 71.28, 71.09, 70.09, 70.07, 70.05, 69.74, 69.32 ($C_{10}H_9$). MS (*m*/*z*, ESI−) 1028.878 (M−). Anal. calcd for $C_{44}H_{30}N_2O_8Fe_2Ru_2$: 1028.880.

[Ru$_3$(CO)$_9$(μ-CO){μ$_2$-η^1:η^1-(4-NH$_2$-PhC(O))CC(Fc)}OC{μ$_3$-η^1:η^2-(Fc)CC(4-NH$_2$-PhC(O))}] (4c). Black powder. Yield: 15%. FT-IR (KBr, cm^{-1}): 3483 m, 3373 m, 2084 vs, 2052 vs, 2021 vs, 1995 vs, 1946 s, 1591 s. ^{1}H NMR (400 MHz, $CDCl_3$) δ 7.70–7.86 (t, 4H, C_6H_4), 6.92 (s, 4H, –NH_2), 6.59–6.72 (m, 4H, C_6H_4), 3.96–4.30 (m, 18H, $C_{10}H_9$). ^{13}C{1H} NMR (101 MHz, $CDCl_3$) δ 197.76, 196.88, 191.59, 191.05 (CO), 174.04, 168.38, 164.55, 159.21 (C≡C), 133.06, 133.05, 132.98, 132.95, 130.27, 129.94, 129.93, 125.16, 122.01, 115.52, 112.77 (C_6H_4), 73.38, 72.07, 72.03, 71.88, 71.76, 71.43, 71.09, 70.91, 70.85, 70.61 ($C_{10}H_9$). MS (*m*/*z*, ESI−) 1241.766 (M−). Anal. calcd for $C_{48}H_{30}N_2O_{12}Fe_2Ru_3$: 1241.763.

[Ru(CO)$_3${μ$_4$-η^1:η^2:η^1:η^1-(Fc)CC(4-NH$_2$-PhC(O))C(4-NH$_2$-PhC(O))C(Fc)Ru(CO)$_3$}μ-CO] (4d). Red-brown powder. Yield: 19%. FT-IR (KBr, cm^{-1}): 3477 m, 3370 m, 3224 w, 2083 vs, 2052 vs, 2020 vs, 1992 vs, 1590 s. ^{1}H NMR (400 MHz, $CDCl_3$) δ 7.70–7.87 (t, 4H, C_6H_4), 6.81–6.92 (d, 4H, –NH_2), 6.59–6.72 (m, 4H, C_6H_4), 4.22–4.94 (m, 18H, $C_{10}H_9$). ^{13}C{1H} NMR (101 MHz, $CDCl_3$) δ 193.62, 191.82, 191.06 (CO), 153.77, 147.81, 146.14 (C≡C), 135.44, 134.53, 133.80, 133.78, 133.75, 133.49, 129.01, 115.50, 115.42, 115.37 (C_6H_4), 74.36, 73.63, 73.09, 72.03, 71.76, 71.43, 71.28, 71.09 ($C_{10}H_9$). MS (*m*/*z*, ESI−) 1031.880 (M−). Anal. calcd for $C_{44}H_{30}N_2O_8Fe_2Ru_2$: 1031.880.

[Ru$_3$(CO)$_9$(μ$_2$-CO){μ$_3$-η^1:η^2:η^1-(4-NO$_2$-PhC(O))CC(Ph)}] (5a). Red-brown powder. Yield: 10%. FT-IR (KBr, cm^{-1}): 3099 w, 2101 vs, 2056 vs, 2032 vs, 1855 m, 1524 s. ^{1}H NMR (400 MHz, $CDCl_3$) δ 8.39–8.48 (dd, 4H, C_6H_4), 3.97–4.28 (m, 18H, $C_{10}H_9$). ^{13}C{1H} NMR (101 MHz, $CDCl_3$) δ 194.11 (CO), 167.96, 165.40 (C≡C), 150.30, 138.52, 131.31, 123.74 (C_6H_4), 95.49, 70.26, 70.17, 70.14, 70.01, 69.88, 69.76, 69.65 ($C_{10}H_9$). MS (*m*/*z*, ESI−) 945.687 (M−). Anal. calcd for $C_{29}H_{13}O_{13}NFeRu_3$: 945.689.

[Ru(CO)$_3${μ$_4$-η^1:η^2:η^1:η^1-(4-NO$_2$-PhC(O))CC(Fc)C(4-NO$_2$-PhC(O))C(Fc)Ru(CO)$_3$}μ-CO] (5b). Red-brown powder. Yield: 17%. FT-IR (KBr, cm^{-1}): 3095 w, 2091 s, 2061 vs, 2022 vs, 1520 s. ^{1}H NMR (400 MHz, $CDCl_3$) δ 8.27–8.32 (t, 4H, C_6H_4), 8.04–8.11 (m, 4H, C_6H_4), 3.94–4.30 (m, 18H, $C_{10}H_9$). ^{13}C{1H} NMR (101 MHz, $CDCl_3$) δ 194.69, 192.60, 192.25 (CO), 150.03 (C≡C), 140.03, 130.65, 130.01, 123.69, 123.41 (C_6H_4), 84.01, 74.02, 71.21, 70.99, 70.69, 69.85, 69.50, 68.83, 68.17 ($C_{10}H_9$). MS (*m*/*z*, ESI−) 1091.826 (M−). Anal. calcd for $C_{44}H_{26}O_{12}N_2Fe_2Ru_2$: 1091.828.

[Ru(CO)$_3${μ$_4$-η^1:η^2:-η^1:η^1-(4-NH$_2$-PhC(O))CC(Ph)C(Ph)C(4-NO$_2$-PhC(O))Ru(CO)$_3$}μ-CO] (5c). Red-brown powder. Yield: 12%. FT-IR (KBr, cm^{-1}): 2091 s, 2055 vs, 2007 vs, 1595 m, 1528 m. ^{1}H NMR (400 MHz, $CDCl_3$) δ 7.77–8.32 (m, 8H, C_6H_4), 6.69–6.80 (dd, 2H, –NH_2), 3.56–4.29 (m, 18H, $C_{10}H_9$). ^{13}C{1H} NMR (101 MHz, $CDCl_3$) δ 197.06 (CO), 151.10 (C≡C), 139.54, 133.12, 130.65, 130.07, 129.90, 123.50, 123.16 (C_6H_4), 71.51, 70.98, 70.69, 70.50, 70.30, 69.85, 69.82, 69.66, 69.15, 68.55, 68.53, 67.41 ($C_{10}H_9$). MS (*m*/*z*, ESI−) 1059.853 (M−). Anal. calcd for $C_{44}H_{28}O_{10}N_2Fe_2Ru_2$: 1059.853.

[Ru(CO)$_3${μ$_4$-η^1:η^2:η^1:η^1-(Fc)CC(4-NH$_2$-PhC(O))C(4-NO$_2$-PhC(O))C(Fc)Ru(CO)$_3$}μ-CO] (5d). Red-brown powder. Yield: 21%. FT-IR (KBr, cm^{-1}): 3481 w, 3343 w, 2087 vs, 2060 vs, 2020 vs, 1993 vs, 1961 vs, 1591 m, 1524 m. ^{1}H NMR (400 MHz, $CDCl_3$) δ 8.23–8.26 (d, 2H, C_6H_4), 7.56–8.04 (m, 6H, C_6H_4), 6.68–6.70 (d, 2H, –NH_2), 3.95–4.25 (m, 18H, $C_{10}H_9$). ^{13}C{1H} NMR (101 MHz, $CDCl_3$) δ 195.43 (CO), 150.78, 149.75 (C≡C), 140.37, 130.62, 128.15, 126.01, 124.64, 124.42, 123.24 (C_6H_4), 73.95, 70.70, 70.56, 70.52, 70.29, 70.13, 69.76, 69.70, 68.75, 68.30, 68.10, 67.36 ($C_{10}H_9$). MS (*m*/*z*, ESI−) 1061.854 (M−). Anal. calcd for $C_{44}H_{28}O_{10}N_2Fe_2Ru_2$: 1061.854.

[Ru$_3$(CO)$_9$(μ$_2$-CO){μ$_3$-η^1:η^2:η^1-(FcC(O))CC(Fc)}] (6a). Red-brown powder. Yield: 29%. FT-IR (KBr, cm^{-1}): 3087 m, 2080 w, 2056 w, 2017 m, 1970 w, 1931 m, 1574 vs, 818 vs. ^{1}H NMR (400 MHz, $CDCl_3$) δ 4.94 (s, 2H, $C_{10}H_9$), 4.84 (s, 2H, $C_{10}H_9$), 4.57 (s, 2H, $C_{10}H_9$), 4.42 (s, 2H, $C_{10}H_9$), 4.35 (s, 5H, $C_{10}H_9$), 4.25 (s, 5H, $C_{10}H_9$). ^{13}C{1H} NMR (101 MHz, $CDCl_3$) δ 193.23, 191.57 (CO), 159.14, 158.20 (C≡C), 84.57, 78.57, 77.05, 76.30, 75.98, 75.67, 70.38, 69.17, 68.78, 68.67, 68.62, 68.50, 68.20, 68.13, 67.87, 67.40, 67.31, 67.29, 67.21, 67.07, 66.87, 66.43, 66.15, 65.59, 65.27, 64.95, 64.50, 63.62 ($C_{10}H_9$). MS (*m*/*z*, ESI−) 1018.749 (M−). Anal. calcd for $C_{33}H_{28}O_{11}Fe_2Ru_3$: 1018.748.

Crystallography

X-ray structural measurements were carried out with a Bruker D8 QUEST with a Photo 100 CMOS detector using graphite monochromated MoKα radiation (λ = 0.71073). The data were collected by the ω–2θ scan mode, and absorption correction was applied by using Multi-Scan. The structure was solved by direct methods (SHELXS-2014/97) and refined by full-matrix least squares against F2 using SHELXL-2014 and SHELXL-97 software.[26] Non-hydrogen atoms were refined with anisotropic thermal parameters. All hydrogen atoms were geometrically fixed and refined using a riding model.

The single crystals of compounds **1b**, **1d**, **2a**, **2b**, **2c**, **2d**, **4a**, **4d** and **5d** suitable for single crystal X-ray diffraction were successfully grown up from their dichloromethane/hexane solutions after slow evaporation at 0–5 °C. Relevant crystallographic data were given in Table S1 in the ESI.†

Conclusions

We obtained a series of new ruthenium clusters by investigating reactions of the ferrocenyl containing 1,3-ynones **1–6** with

$Ru_3(CO)_{12}$. Some new clusters with unexpected structures were isolated while some anticipated products were not formed, although most of the clusters exhibit a similar skeleton to those of the products *via* reaction of 1,3-diphenylprop-2-yn-1-one derivatives with $Ru_3(CO)_{12}$. An electron-withdrawing group at the carbonyl side of an alkynyl ketone is beneficial to the formation of normal ruthenoles **b**, **c** and **d**; while an electron-donating group favors the production of normal ruthenoles **b** and **d**, but disfavors the formation of ruthenole **c**; the larger steric hindrance and electron-donating effect of two ferrocenyl groups in **6** prefers only the formation of **6a**. In addition, we believe that the reduction of half of the nitro groups in both **5c** and **5d** was driven by both the electron-donating ferrocenyl group and CO in the presence of the catalyst $Ru_3(CO)_{12}$. No formation of the expected cyclotrimerization products of the 1,3-ynones can also be ascribed to the unusual properties of the ferrocenyl groups in **1–6**. The reaction between $Ru_3(CO)_{12}$ and a 1,3-ynone with a ferrocenyl group at its C≡C side has given some unexpected results, which promotes us to investigate the reaction of $Ru_3(CO)_{12}$ with alkynyl ketones containing ferrocenyl groups at their carbonyl sides; this study is already underway.

Computational details

The optimization used DFT method with the Becke's three parameter hybrid functional and Lee Yang Parr's gradient corrected correlation functional (B3LYP).[27] Calculations were performed with the GAUSSIAN-09 program.[28] The LanL2DZ basis set and effective core potential were used for the Fe and Ru atoms, and the 6-31G basis sets were used for all other atoms, respectively.[29] The nature of all stationary points were confirmed by performing a normal-mode analysis. The input model molecules for **5c** and the predicted **5c′** were based on the head-to-head coupled ruthenoles we reported earlier[17] and the structure of **2c** was also optimized.

Conflicts of interest

No conflicts of interest to declare.

Acknowledgements

This work is supported by the National Natural Science Foundation of China (21401124 and 21171112).

Notes and references

1 (*a*) S. Ko, Y. Na and S. Chang, *J. Am. Chem. Soc.*, 2002, **124**, 750; (*b*) F. Kakiuchi, K. Tsuchiya, M. Matsumoto, E. Mizushima and N. Chatani, *J. Am. Chem. Soc.*, 2004, **126**, 12792; (*c*) C. S. Yi, S. Y. Yun and I. A. Guzei, *J. Am. Chem. Soc.*, 2005, **127**, 5782; (*d*) M. Nishiumi, H. Miura, K. Wada, S. Hosokawa and M. Inoue, *Adv. Synth. Catal.*, 2010, **352**, 3045; (*e*) M. Kawatsura, M. Yamamoto, J. Namioka, K. Kajita, T. Hirakawa and T. Itoh, *Org. Lett.*, 2011, **13**, 1001; (*f*) K. Takahashi, M. Yamashita and K. Nozaki, *J. Am. Chem. Soc.*, 2012, **134**, 18746; (*g*) E. L. McInturff, J. Mowat, A. R. Waldeck and M. J. Krische, *J. Am. Chem. Soc.*, 2013, **135**, 17230; (*h*) L. P. Wu, I. Fleischer, R. Jackstell, I. Profir, R. Franke and M. Beller, *J. Am. Chem. Soc.*, 2013, **135**, 14306; (*i*) E. L. McInturff, J. Mowat, A. R. Waldeck and M. J. Krische, *J. Am. Chem. Soc.*, 2014, **135**, 3796; (*j*) B. Li, I. Park and S. Chang, *J. Am. Chem. Soc.*, 2014, **136**, 1125; (*k*) W. J. Park, C. H. Lee, D. S. Kim and C. H. Jun, *Chem. Commun.*, 2015, **51**, 14667; (*l*) A. Saxena, F. Perez and M. J. Krische, *Angew. Chem., Int. Ed.*, 2016, **55**, 1493; (*m*) W. Li, X. Huang and J. You, *Org. Lett.*, 2016, **18**, 666.

2 (*a*) J. Liu, C. Kubis, R. Franke, R. Jackstell and M. Beller, *ACS Catal.*, 2016, **6**, 907; (*b*) Z. Fan, J. Ni and A. Zhang, *J. Am. Chem. Soc.*, 2016, **138**, 8470; (*c*) Y. Yuki, K. Takahashi, Y. Tanaka and K. Nozaki, *J. Am. Chem. Soc.*, 2013, **135**, 17393; (*d*) N. Armanino, M. Lafrance and E. M. Carreira, *Org. Lett.*, 2014, **16**, 572; (*e*) S. T. Tan, J. W. Kee and W. Y. Fan, *Organometallics*, 2011, **30**, 4008; (*f*) X. Guo and C. J. Li, *Org. Lett.*, 2011, **13**, 4977.

3 (*a*) C. E. Ellul, J. P. Lowe, M. F. Mahon, P. R. Raithby and M. K. Whittlesey, *Dalton Trans.*, 2018, **47**, 4518; (*b*) J. Yan, Z. Han, D. Zhang and C. Liu, *RSC Adv.*, 2016, **6**, 99625; (*c*) J. A. Cabeza, M. Damonte, P. García -Álvareza and E. Pérez-Carreño, *Chem. Commun.*, 2013, **49**, 2813; (*d*) J. A. Cabeza, M. Damonte, P. García-Álvarez, M. G. Hernández-Cruz and A. R. Kennedy, *Organometallics*, 2012, **31**, 327; (*e*) J. A. Cabeza, M. Damonte and E. Pérez-Carreño, *Organometallics*, 2012, **31**, 8114; (*f*) J. A. Cabeza, M. Damonte and E. Pérez-Carreño, *Organometallics*, 2012, **31**, 8355; (*g*) J. A. Cabeza, M. Damonte, P. García-Álvareza, A. R. Kennedy and E. Pérez-Carreño, *Organometallics*, 2011, **30**, 826.

4 (*a*) B. Li, X. Tan, S. Xu, H. Song and B. Wang, *J. Organomet. Chem.*, 2009, **694**, 1503; (*b*) P. Ghosh, P. J. Fagan, W. J. Marshall, E. Hauptman and R. M. Bullock, *Inorg. Chem.*, 2009, **48**, 6490; (*c*) K. Xu, B. Li, S. Xu, H. Song and B. Wang, *Organometallics*, 2009, **28**, 4438; (*d*) S. Ngubane, M. Hakansson, S. Jagner, J. R. Moss and A. Sivaramakrishna, *J. Organomet. Chem.*, 2008, **693**, 343; (*e*) B. Li, B. Wang, S. Xu, X. Zhou and H. Song, *Organometallics*, 2012, **31**, 8114; (*f*) J. A. Cabeza, M. Damonte and E. Pérez-Carreño, *Organometallics*, 2006, **25**, 1158.

5 T. Takao, M. Moriya and H. Suzuki, *Organometallics*, 2008, **27**, 1044.

6 M. Akita, S. Sugimoto, H. Hirakawa, S. Kato, M. Terada, M. Tanaka and Y. Moro-oka, *Organometallics*, 2001, **20**, 1555.

7 (*a*) H. Sato, M. Bender, W. J. Chen and M. J. Krische, *J. Am. Chem. Soc.*, 2016, **138**, 16244; (*b*) J. P. Hopewell, J. E. D. Martins, T. C. Johnson, J. Godfrey and M. Wills, *Org. Biomol. Chem.*, 2012, **10**, 134; (*c*) M. Kawatsura, M. Yamamoto, J. Namioka, K. Kajita, T. Hirakawa and T. Itoh, *Org. Lett.*, 2011, **13**, 1001.

8 (*a*) M. Krempe, R. Lippert, F. Hampel, I. Ivanovic-Burmazovic, N. Jux and R. R. Tykwinski, *Angew. Chem., Int. Ed.*, 2016, **55**, 14802; (*b*) C. Cesari, L. Sambri, S. Zacchini, V. Zanotti and R. Mazzoni, *Organometallics*, 2014, **33**, 2814;

(*c*) H. Masai, J. Terao, S. Seki, S. Nakashima, M. Kiguchi, K. Okoshi, T. Fujihara and Y. Tsuji, *J. Am. Chem. Soc.*, 2014, **136**, 1742.

9 (*a*) E. Sappa, A. Tiripicchio and P. Braunstein, *Chem. Rev.*, 1983, **83**, 203; (*b*) M. J. Rosales and P. R. Raithby, *Adv. Inorg. Chem. Radiochem.*, 1985, **29**, 169.

10 P. J. Low, G. D. Enright and A. J. Carty, *J. Organomet. Chem.*, 1998, **565**, 279.

11 S. W. Lau and W. Wong, *J. Chem. Soc., Dalton Trans.*, 1999, **15**, 2511–2519.

12 R. Rosseto and M. D. Vargas, *J. Organomet. Chem.*, 2004, **689**, 111.

13 M. Li, H. Song, S. Xu and B. Wang, *Organometallics*, 2010, **29**, 6092.

14 P. Mathur, D. K. Rai, R. K. Joshi, B. Jha and S. M. Mobin, *Organometallics*, 2014, **33**, 3857.

15 (*a*) S. V. Osintseva, F. M. Dolgushin, N. A. Shtel'tser, P. V. Petrovskii, A. Z. Kreindlin, L. V. Rybin and M. Y. Antipin, *Organometallics*, 2005, **24**, 2279; (*b*) W. K. Tsui, L. H. Chung, W. H. Tsang, C. F. Yeung, C. H. Chiu, H. S. Lo and C. Y. Wong, *Organometallics*, 2015, **34**, 1005; (*c*) B. F. G. Johnson, J. M. Matters, P. E. Gaede, S. L. Ingham, N. Choi, M. M. Partlin and M. A. Pearsall, *J. Chem. Soc., Dalton Trans.*, 1997, 3251.

16 (*a*) N. Arai, H. Satoh, N. Utsumi, K. Murata, K. Tsutsumi and T. Ohkuma, *Org. Lett.*, 2013, **15**, 3030; (*b*) W. P. Unsworth, J. D. Cuthbertson and R. J. K. Taylor, *Org. Lett.*, 2013, **15**, 3306; (*c*) J. Shen, G. Cheng and X. Cui, *Chem. Commun.*, 2013, **49**, 10641; (*d*) M. Yoshida, K. Saito, Y. Fujino and T. Doi, *Chem. Commun.*, 2012, **48**, 11796; (*e*) B. H. Xu, G. Kehr, R. Froehlich, B. Wibbeling, B. Schirmer, S. Grimme and G. Erker, *Angew. Chem., Int. Ed.*, 2011, **50**, 7183.

17 (*a*) J. Yang, W. Zhang, G. Zhang and Z. Gao, *J. Organomet. Chem.*, 2015, **799**, 166; (*b*) L. Xu, S. Li, L. Jiang, G. Zhang, W. Zhang and Z. Gao, *RSC Adv.*, 2018, **8**, 4354.

18 X. M. Chen and J. W. Cai, In *Single-Crystal Structural Analysis-Principles and Practices*, Science China Press, Beijing, China, 2nd edn, 2004, p. 114.

19 (*a*) A. J. Arce, P. Arrojo, A. J. Deeming and Y. De Sanctis, *Dalton Trans.*, 1992, **15**, 2423; (*b*) A. J. Arce, R. Machado, C. Rivas, Y. De Sanctis and A. J. Deeming, *J. Organomet. Chem.*, 1991, **419**, 63.

20 (*a*) V. V. Krivykh, O. A. Kizas, E. V. Vorontsov, F. M. Dolgushin, A. I. Yanovsky, Y. T. Struchkov and A. A. Koridze, *J. Organomet. Chem.*, 1996, **508**, 39; (*b*) A. J. Amoroso, L. P. Clarke, J. E. Davies, J. Lewis, H. R. Powell, P. R. Raithby and G. P. Shields, *J. Organomet. Chem.*, 2001, **635**, 119; (*c*) G. Gervasio, *J. Chem. Soc., Chem. Commun.*, 1976, **1**, 25.

21 R. S. Dickson and B. C. Greaves, *Organometallics*, 1993, **12**, 3249.

22 T. Takahashi, Z. Xi, A. Yamazaki, Y. Liu, K. Nakajima and M. Kotora, *J. Am. Chem. Soc.*, 1998, **120**, 1672.

23 (*a*) A. Bassoli, B. Rindone, S. Tollari, S. Cenini and C. Crotti, *J. Mol. Catal.*, 1990, **60**, 155; (*b*) A. Thurkauf, B. de Costa, P. Berger, S. Paulz and K. C. Rice, *J. Labelled Compd. Radiopharm.*, 1991, **2**, 126.

24 M. Lauwiner, R. Roth and P. Rys, *Appl. Catal., A*, 1999, **177**, 9.

25 B. Yu, H. Sun, Z. Xie, G. Zhang, L. Xu, W. Zhang and Z. Gao, *Org. Lett.*, 2015, **17**, 3298.

26 G. M. Sheldrick, *Acta Crystallogr., Sect. A: Found. Crystallogr.*, 2008, **A64**, 112.

27 P. J. Stephens, F. J. Devlin, C. F. Chabalowski and M. J. Frisch, *J. Phys. Chem.*, 1994, **98**, 11623.

28 M. Frisch, G. Trucks, K. Schlegel and G. Scuseria, *et al.*, *Gaussian 09, Revision A.02*, Gaussian, Inc, 2009.

29 P. J. Hay and W. R. Wadt, *J. Chem. Phys.*, 1985, **82**, 270.